ACS APPLIED MATERIALS & INTERFACES

www.acsami.org

Research Article

Facile Preparation of Hydrogel-Coated Surfaces with Antifouling and Salt Resistance for Efficient Solar-Driven Water Evaporation

Xingzhen Zhang, Shouyong Zhou, Zhigang Wang, Xian Wei, Shenxiang Zhang,* and Jian Jin

Cite This: https://doi.org/10.1021/acsami.3c11299

Read Online

ACCESS | Metrics & More | Article Recommendations | Supporting Information

ABSTRACT: Hydrogel-based evaporators are a promising strategy to obtain freshwater from seawater and sewage. However, the time-consuming and energy-consuming methods used in hydrogel preparation, as well as their limited scalability, are major factors that hinder the development of a hydrogel-based evaporator. Herein, a facile and scalable strategy was designed to prepare a hydrogel-coated evaporator to realize efficient solar-driven water evaporation. The hydrogel coating layer is composed of a robust 3D network formed by tannic acid (TA) and poly(vinyl alcohol) (PVA) through a hydrogen bond. With the assistance of TA surface modifier, carbon black (CB) is uniformly distributed within the hydrogel matrix, endowing the coating with remarkable photothermal properties. In addition, Fe^{3+} is deposited on the surface of the hydrogel coating through metal coordination with TA, further improving the light absorption of the coating. Due to the synergistic effect of CB and Fe^{3+}, the hydrogel-coated foam exhibited excellent photothermal properties. The water evaporation rate reached 3.64 kg m^{-2} h^{-1} under 1 sun irradiation. Because of the hydration ability of PVA hydrogel and the large porous structure of the foam, the hydrogel-coated foam demonstrated excellent antifouling performance and salt resistance. This study provides a facile method for designing and manufacturing high-performance solar-driven water evaporation materials.

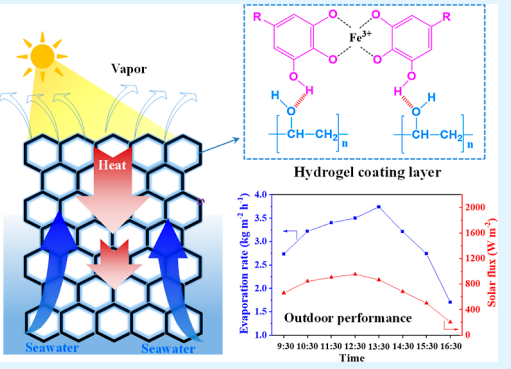

KEYWORDS: *solar-driven water evaporation, hydrogel, antifouling, salt resistance, photothermal property*

1. INTRODUCTION

The lack of access to clean and fresh water is a pressing issue that poses a serious challenge to the world. Even though approximately 70% of the earth's surface is covered by water, the availability of freshwater resources that sustain human life is alarmingly low.[1,2] In order to alleviate the shortage of fresh water, various advanced technologies for extracting fresh water from seawater or sewage have been developed, such as distillation, reverse osmosis, and electrodialysis.[3−5] However, these technologies usually require high energy consumption and high costs. Solar-driven water evaporation, which utilizes solar energy to obtain clean water, is a promising strategy to provide solutions for freshwater shortages due to its high efficiency, low cost, simple equipment, and environment-friendly nature.[6,7]

Salt resistance and antifouling are two key parameters affecting the efficient application of a solar-driven evaporator in practical, complex environments.[8,9] In the long-term evaporation process, the salt at the interface cannot diffuse to the underlying water in time and will gradually deposit on the surface of the photothermal material, which not only weakens the evaporation rate of water but also affects the service life of materials.[10−12] At the same time, during the treatment of oil-contaminated seawater or oily wastewater such as oil/water emulsions, oil can block water channels and decrease the evaporation efficiency, which greatly affects the practical application of evaporators to extract freshwater from seawater or sewage.[13,14] Therefore, it is highly desirable to design evaporators with high evaporation efficiency and long-term salt and oil resistance.

Hydrogel, consisting of 3D cross-linked polymeric networks, has been widely used in various applications due to its high porosity, adjustable porous structure, and super hydrophilicity.[15−18] Photothermal material is dispersed into hydrogel to form hydrogel-based evaporators, where hydrogel endows evaporators with antifouling and salt resistance, and photothermal material endows them with a high evaporation rate.[19] Therefore, hydrogel-based evaporators have been recognized as one of the most promising technologies for solar-driven water evaporation.[6,20,21] Zhao et al. prepared the hydrogel evaporator by freezing and thawing poly(vinyl alcohol) (PVA) and polypyrrole (PPy). The solar energy absorbed by PPy can be used locally to drive the evaporation of water contained in

Received: July 31, 2023
Accepted: October 10, 2023

the PVA molecular grid. At the same time, the framework of hydrogel promotes water evaporation, thus obtaining high evaporation efficiency.[22] Xu et al. prepared a chitosan/PAAm/PPy gradient structure hydrogel evaporator, which showed good self-cleaning performance, salt deposition resistance, and bacterial growth prevention performance. Under 1 sun irradiation, the evaporation rate can reach 2.41 kg m^{-2} h^{-1}.[23]

Although various hydrogel-based evaporators have been designed and great achievements have been made, challenges still exist. A hydrogel evaporator is typically produced using the freezing-thawing method, which can be both time-consuming and energy-consuming.[24] Besides, the preparation of a hydrogel-based evaporator involves the incorporation of photothermal materials, such as plasma,[25] semiconductor,[26−28] and carbon-containing materials.[29−32] These materials usually do not disperse well and are prone to aggregation within solvents, which can lead to compatibility issues between photothermal materials and hydrogel and ultimately impact the evaporation efficiency of the system.

To improve the dispersibility of photothermal materials in the hydrogel, tannic acid (TA), a natural polyphenol compound, was selected as a modifier. PVA was used in the fabrication of hydrogel, owing to the strong hydrogen bonds that can be formed between TA and PVA. To avoid the time-consuming and energy-consuming nature of the traditional freezing-thawing method, we propose a hydrogel-coated melamine foam as an evaporator to realize efficient water evaporation. The coating consists of a 3D hydrogel network formed by TA, CB, and PVA through hydrogen bonds. Additionally, Fe^{3+} is deposited on the surface through metal coordination. Due to the synergistic effect of CB and Fe^{3+}, the hydrogel-coated foam could efficiently capture sunlight and convert solar energy into heat energy. The hydrogel network and foam skeleton ensured the continuous supply and rapid transportation of water. Therefore, the hydrogel-coated foam exhibits excellent photothermal properties. Moreover, due to the hydration ability of PVA hydrogel and the high porosity of the foam, the hydrogel-coated foam shows excellent antifouling and salt resistance. This study provides a new direction in the fabrication of solar-driven evaporators with excellent antifouling and salt resistance for extracting fresh water from complex practical conditions.

2. EXPERIMENTAL SECTION

2.1. Materials. PVA (224) was provided by Shanghai Meryer Chemical Technology Co., Ltd. Tannic acid (TA) was supplied by Shanghai Macklin Biochemical Technology Co., Ltd. Carbon black (CB S.A.75 m^2/g) was purchased from Alfa Aesar A Johnson Matthey Company. Isooctane was obtained from Aladdin Chemistry Co., Ltd. NaCl (AR), $FeCl_3 \cdot 6H_2O$ (AR), and anhydrous alcohol were procured from Sinopharm Chemical Reagent Co., Ltd. Melamine foam was obtained from a local market.

2.2. Instruments and Characterization. The Hitachi Regulus 8230 scanning microscope was used to record the micromorphology and energy-dispersive spectroscopy analysis of hydrogel-coated foams. The OCA20 system (Data-Physics, Germany) was utilized to characterize the underwater−oil contact angle and oil adhesive test of the foams. Optical photographs were taken with a Novel MV6100 microscope. The PerkinElmer Lambda 25 spectrometer was utilized to evaluate the light absorption spectra of the foams. A differential scanning calorimeter (DSC, Netzsch STA 449F3, Germany) was used to test the heat flow−temperature curves of the foams. The dynamic surface temperature was recorded by a thermal infrared imager (ICI 8320, America).

2.3. Fabrication of Hydrogel-Coated Foams. The hydrogel-coated foams were fabricated via a a two-step immersion technique. The preparation of the PVA/CB/TA immersion solution: 1.0 g of TA and a certain amount of CB were added to 17.5 mL of ethanol and 17.5 mL of deionized water. After shaking with ultrasound for 1 h, 1.0 g of PVA was added and stirred at 90 °C for 6 h to obtain a homogeneous solution. The preparation of $FeCl_3$ immersion solution: 2% $FeCl_3 \cdot 6H_2O$ was dissolved in water and stirred for 1 h to obtain a homogeneous solution. The two-step immersion process is as following: First, the melamine foam (1.5 cm × 1.5 cm × 1.5 cm) was thoroughly washed by deionized water and ethanol to remove impurities, and then, was dried for use. The as-prepared foam was immersed in a PVA/CB/TA solution for 1 min and dried in air to obtain a PVA/CB/TA-coated foam. Then, the foam was immersed in $FeCl_3$ solution for 1 h. After washing for 24 h, PVA/CB/TA/Fe^{3+}coating foam was fabricated. The obtained foam is denoted as PVA/CB-*x*/TA/Fe^{3+}-coated foam (*x* means the amount of CB). When *x* is not marked, the added amount of CB is 0.1 g.

2.4. Water Evaporation Test of Hydrogel-Coated Foams. The water evaporation experiment was carried out on the self-made device (Figure S1a) using simulated sunlight provided by the solar simulator (PL-X300DF), with a temperature of 25 °C and a humidity of 40%. The light intensity was 1 kW m^{-2}. The hydrogel-coated foam was placed on the device as shown in Figure S1b, and the real-time mass change was recorded by the electronic balance. The water evaporation rate (V, kg m^{-2} h^{-1}) was calculated by the following formula[30]

$$V = \frac{\Delta m}{S \times \Delta t} \tag{1}$$

where Δm (kg) means the mass change during evaporation, S (m^2) represents the effective evaporation area, and Δt (h) means the evaporation time.

3. RESULTS AND DISCUSSION

3.1. Preparation and Characterization of Hydrogel-Coated Foam. The hydrogel-based evaporator usually involves a photothermal material within the hydrogel matrix. Therefore, achieving an even dispersion of photothermal material is crucial to ensuring optimal performance. As shown in Figure S2a, after ultrasonic and high-speed stirring, most CB floats on the surface and cannot be well dispersed in water. The water contact angle of the unmodified CB is 141°, which shows hydrophobicity. After adding TA in the solution, CB can be uniformly dispersed to the solution (Figure S2b). The contact angle of the modified CB is 0°, which shows superhydrophilicity. TA boasts an abundance of phenolic hydroxyl groups that are capable of physically or chemically interacting with a wide range of groups. This unique attribute significantly enhances the material's wettability.

PVA hydrogel demonstrates great application potential in solar-driven water evaporation due to its good biocompatibility, hydrophilicity, and mechanical properties.[33−36] However, the PVA hydrogel is usually prepared by the freezing-thawing method, which is time-consuming and energy-consuming. The strong hydrogen bonding between PVA and TA provides a facile method to cross-link PVA into hydrogel.[37] As shown in Figure S3a, the gelatinous precipitates were generated when TA and PVA were mixed together. However, when some ethanol was introduced into the solution, the formation of gelatinous precipitates was prevented (Figure S3b). The addition of ethanol can weaken the hydrogen bond cross-linking between TA and PVA, thereby obtaining a stable and uniform solution.[38] When the ethanol molecule is removed, the hydrogen bond between the molecules is

https://doi.org/10.1021/acsami.3c11299
ACS Appl. Mater. Interfaces XXXX, XXX, XXX−XXX

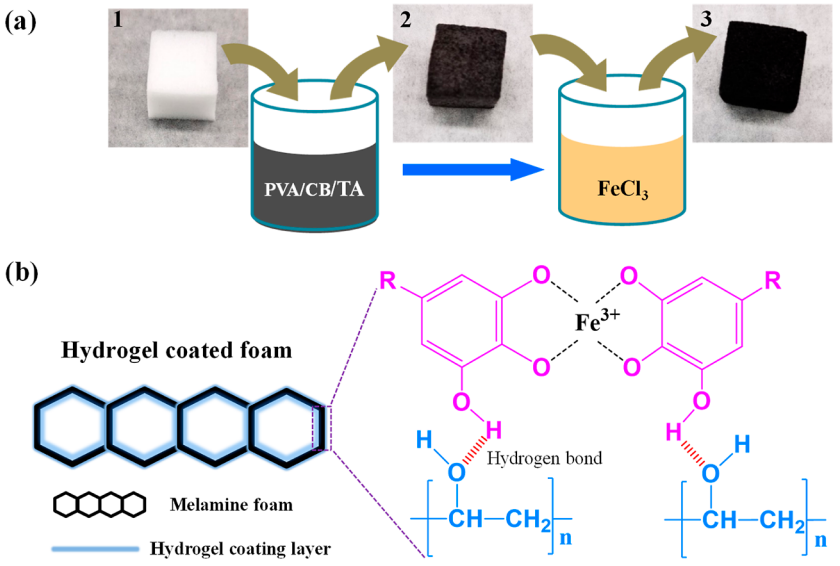

Figure 1. (a) Schematic fabrication of the hydrogel-coated foam. Photographs of (sample 1) pristine foam, (sample 2) PVA/CB/TA-coated foam, and (sample 3) PVA/CB/TA/Fe^{3+}-coated foam. (b) Schematic mechanism of the hydrogel-coated foam.

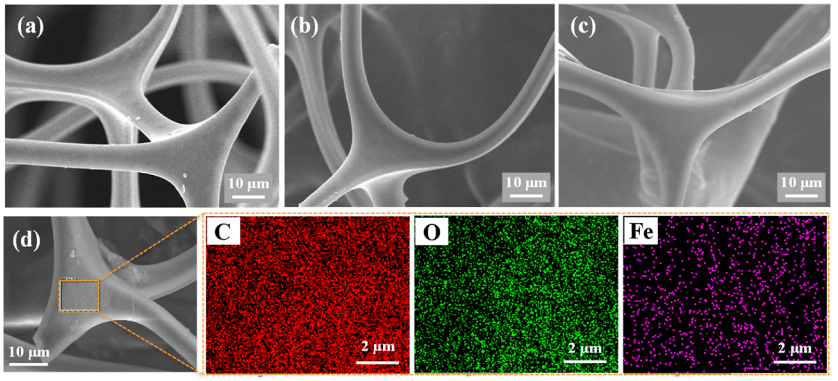

Figure 2. SEM images of (a) pristine foam, (b) PVA/CB/TA-coated foam, and (c) PVA/CB/TA/Fe^{3+}-coated foam. (d) Elemental mapping images of the PVA/CB/TA/Fe^{3+}-coated foam.

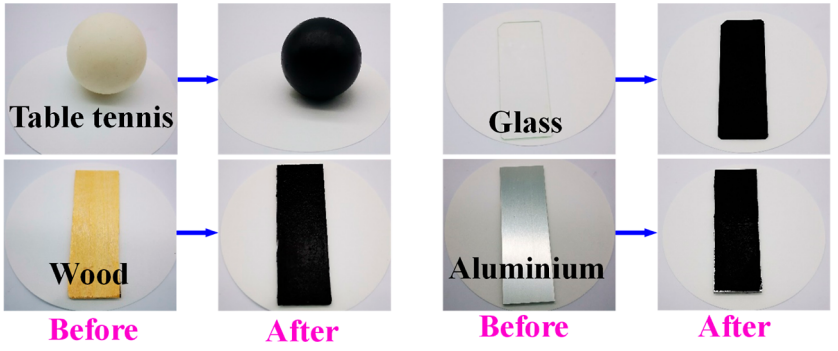

Figure 3. Photographs of materials before and after hydrogel coating.

restored so that a hydrogel coating can be generated in situ on the surface of the substrate.

For this reason, TA and CB were first dispersed in an ethanol/water solution with a 1:1 volume. After ultrasonication, PVA was added to the above solution to obtain the uniformly dispersed hydrogel solution. As shown in Figure 1a, the pristine melamine foam was dipped in the above hydrogel solution to obtain PVA/CB/TA-coated foam. After drying in air, the foam was then immersed in $FeCl_3$ solution to obtain the PVA/CB/TA/Fe^{3+}-coated foam. The color of pristine foam is white, and it turns gray-black after dipping in the hydrogel solution. At last, the foam becomes dark black after immersing in the $FeCl_3$ solution, which intuitively indicates that the hydrogel is successfully coated on the foam. The schematic mechanism of the hydrogel-coated foam is shown in Figure 1b. The cross-linked hydrogel is formed due to the strong hydrogen bond between TA and PVA. As TA and PVA have ideal adhesion properties, the hydrogel coating can

https://doi.org/10.1021/acsami.3c11299
ACS Appl. Mater. Interfaces XXXX, XXX, XXX−XXX

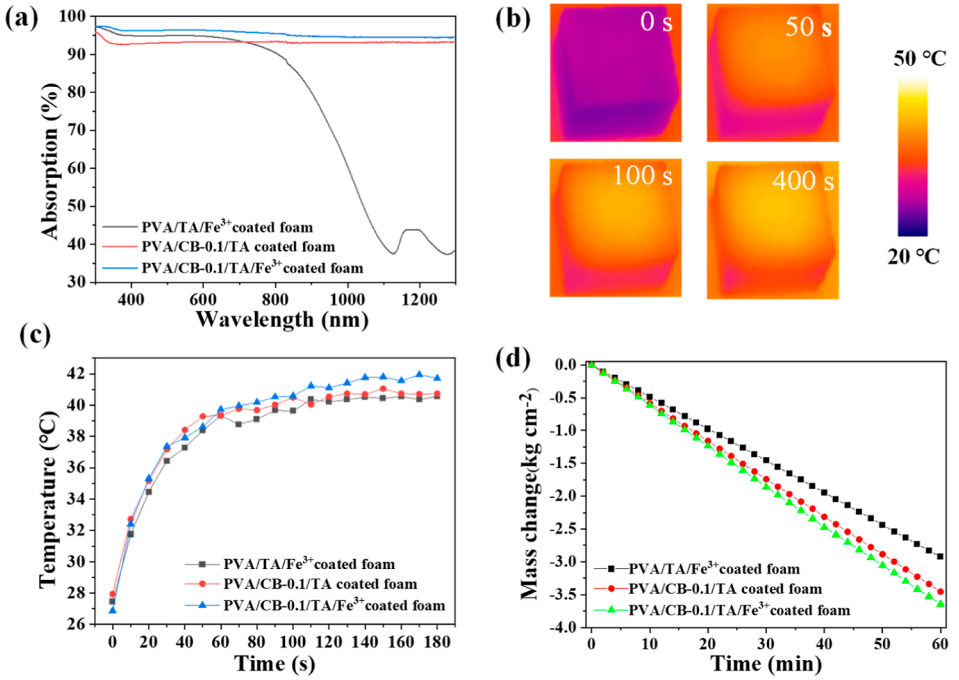

Figure 4. (a) Light absorption spectra of PVA/TA/Fe^{3+}-, PVA/CB-0.1/TA-, and PVA/CB-0.1/TA/Fe^{3+}-coated foams. (b) Infrared images of PVA/CB-0.1/TA/Fe^{3+}-coated foam at different times under 1 sun irradiation. (c) Surface temperature changes of PVA/TA/Fe^{3+}-, PVA/CB-0.1/TA-, and PVA/CB-0.1/TA/Fe^{3+}-coated foams during 3 min of irradiation. (d) Mass change curve of PVA/TA/Fe^{3+}-, PVA/CB-0.1/TA-, and PVA/CB-0.1/TA/Fe^{3+}-coated foams under 1 sun irradiation.

firmly adhere to the foam surface. In addition, due to the metal coordination effect between TA and Fe^{3+}, Fe^{3+} can be deposited on the surface of the hydrogel coating.

The scanning electron microscopy (SEM) images of the foams before and after coating are shown in Figure 2. Compared with the pristine foam (Figure 2a), a thin coating layer is found on the surface after the immersion of the hydrogel (Figure 2b). The surface morphology of the foam does not change significantly after further immersion in Fe^{3+} (Figure 2c). These results show that the hydrogel layer is successfully formed on the surface of the foam. The elemental mapping images of PVA/CB/TA/Fe^{3+}-coated foam were collected (Figure 2d). C, O, and Fe elements can be clearly found on the coating surface, indicating that Fe^{3+} and CB are successfully loaded onto the foam surface. The surface chemistry of PVA/CB/TA/Fe^{3+}-coated foam was also studied by XPS (Figure S4), which further confirmed that the coating contained C, O, and Fe^{3+}.

With a multitude of phenolic hydroxyl groups and hydroxyl groups, TA and PVA have the ability to bond with various materials through hydrogen bonding. Therefore, the hydrogel coating obtained by this method can adhere to the surface of a variety of materials, such as plastic, wood, glass, and metal materials. As shown in Figure 3, the surface of ping-pong ball, wood, glass and aluminum becomes uniformly black after the two-step immersion process, indicating that the hydrogel coating is successfully modified on the surface of these materials. Therefore, this strategy provides a facile method for the preparation and design of hydrogel coating layers.

3.2. Effect of CB and Fe^{3+} on the Photothermal Performance of the Evaporator. CB plays a decisive role in the photothermal performance of hydrogel-based evaporators. Therefore, it is necessary to optimize the content of CB in the coating. By comparing the light absorption spectra and water evaporation rate of PVA/CB/TA-coated foams with varying levels of CB content, it has been determined that the CB content of 0.1 g is ideal for the following test (Figure S5). TA can react with Fe^{3+} to form coordination compounds through metal ion chelation and endows the material with strong light absorption capacity, which contributes to the photothermal property of the material.[39,40] Therefore, the effects of Fe^{3+} on the light absorption and water evaporation properties of the foams were investigated. As shown in Figure 4a, the light absorption of the PVA/CB-0.1/TA/Fe^{3+}-coated foam is 94.5%, with the maximum light absorption. PVA/CB-0.1/TA-coated foam is 93%, so the introduction of Fe^{3+} improves the light absorption of the foam. Between 300 and 700 nm, the light absorption of PVA/TA/Fe^{3+}-coated foam is higher than that of PVA/CB-0.1/TA, but lower than PVA/CB-0.1/TA/Fe^{3+}. After 700 nm, the light absorption of PVA/TA/Fe^{3+}-coated foam is significantly reduced, which is much lower than that of PVA/CB-0.1/TA and PVA/CB-0.1/TA/Fe^{3+}.

In order to evaluate the photothermal conversion performance, the dynamic surface temperature changes of hydrogel-coated foams under 1 sun irradiation were recorded with an infrared camera. As shown in Figure 4b, the surface temperature of the PVA/CB-0.1/TA/Fe^{3+}-coated foam rapidly increased, reaching 41.9 °C within 400 s, which reflects excellent photothermal conversion performance. Compared with PVA/CB-0.1/TA- and PVA/TA/Fe^{3+}-coated foams, PVA/CB-0.1/TA/Fe^{3+} has the highest surface temperature (Figure 4c). Therefore, Fe^{3+} and CB together achieve efficient light adsorption and photothermal conversion performance in the hydrogel-based evaporator.

The water evaporation performance of the foams is shown in Figure 4d. The PVA/CB-0.1/TA/Fe^{3+}-coated foam maintains the maximum water evaporation rate, followed by PVA/CB-0.1/TA-coated foam, and then PVA/TA/Fe^{3+}-coated foam.

https://doi.org/10.1021/acsami.3c11299
ACS Appl. Mater. Interfaces XXXX, XXX, XXX−XXX

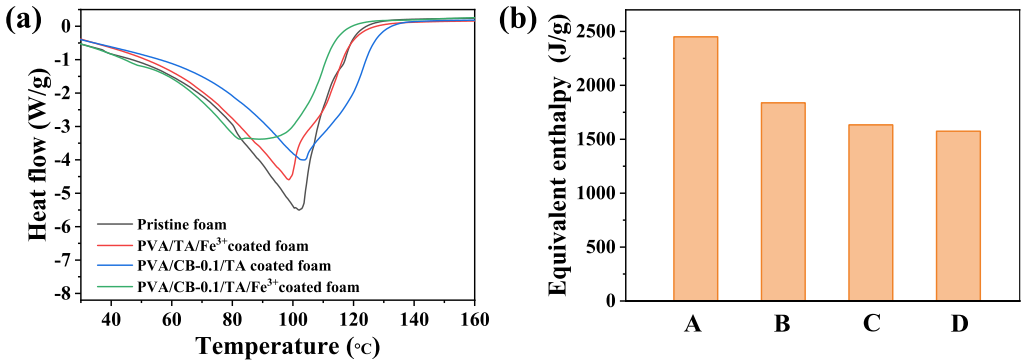

Figure 5. (a) Heat flow−temperature curves of pristine, PVA/TA/Fe^{3+}-, PVA/CB-0.1/TA-, and PVA/CB-0.1/TA/Fe^{3+}-coated foams. The foam sample was put in an open crucible and heated from 20 to 160 °C (heating rate 5 °C/min) under a nitrogen flow rate of 20 mL/min. (b) Equivalent evaporation enthalpies of the foams. Sample A: pure water; Sample B: PVA/TA/Fe^{3+}-coated foam; Sample C: PVA/CB-0.1/TA-coated foam; and Sample D: PVA/CB-0.1/TA/Fe^{3+}-coated foam.

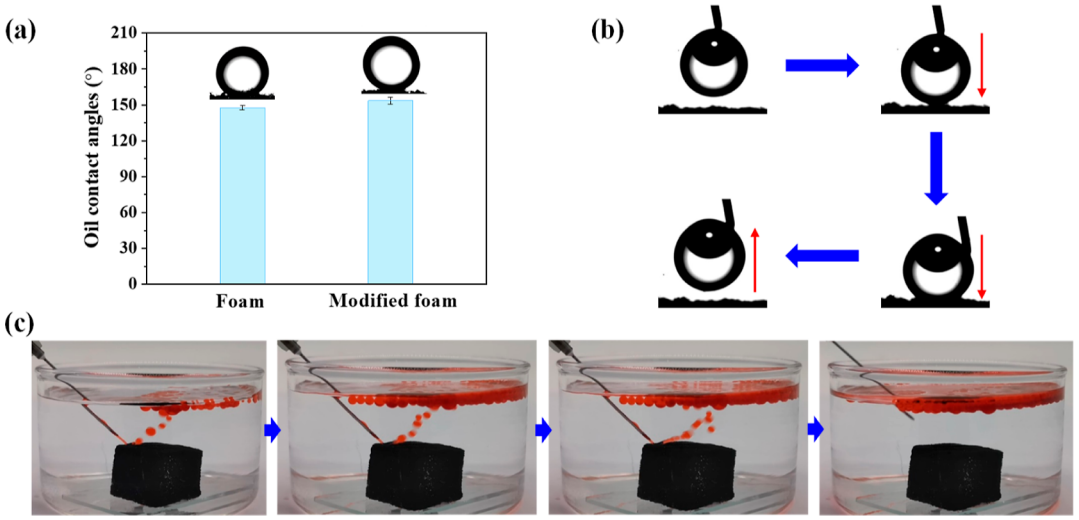

Figure 6. (a) Underwater−oil content angle of pristine foam and PVA/CB/TA/Fe^{3+}-coated foam. (b) Underwater−oil adhesive test and (c) antioil-fouling test of PVA/CB/TA/Fe^{3+}-coated foam.

The water evaporation rates are 3.64, 3.45, and 2.93 kg m^{-2} h^{-1}, respectively. Therefore, the introduction of Fe^{3+} improves the light absorption and water evaporation properties of the foam. This can be explained by the fact that Fe^{3+} and CB have synergistic effects on the photothermal properties of the hydrogel coating. On the one hand, Fe^{3+} is dispersed on the surface of the hydrogel, which increases the light absorption of the coating and realizes the efficient capture of sunlight. On the other hand, CB is dispersed in the hydrogel network, so the absorbed heat energy is used directly to drive the evaporation of water contained in the hydrogel network, thus reducing the energy loss.

The evaporation enthalpy of water in the foams was calculated by DSC measurements.[41,42] As shown in the heat flow−temperature curves (Figure 5a), the curve peak of the pristine foam is significantly bigger than that of hydrogel-coated foams. The evaporation enthalpy can be calculated by integrating the area of the curves. Compared with the pristine foam, the hydrogel-coated foams show a reduced evaporation enthalpy (Table S1). However, DSC can only qualitatively evaluate the reduction in evaporation enthalpy of hydrogel-coated foams. The equivalent evaporation enthalpy only involves the evaporation process of free water and intermediate water, which shows a more realistic evaporation enthalpy of water in hydrogel-coated foams (calculation process shown in Supporting Information note 1). As shown in Figure 5b, the equivalent evaporation enthalpy of pure water, PVA/TA/Fe^{3+}-coated foam, PVA/CB-0.1/TA-coated foam, and PVA/CB-0.1/TA/Fe^{3+}-coated foam is 2450 J/g, 1838 J/g, 1633 J/g, and 1575 J/g, respectively, which has the same trend with the evaporation enthalpy by DSC. Hydrogel-coated foams may contain more intermediate water, which can cause the water to be released from the polymer network in clusters rather than as individual molecules. As a result, the water evaporates with less energy compared to traditional latent heat (for a detailed discussion, see Supporting Information note 2). At the same time, CB and Fe^{3+} are contained in the hydrogel network; therefore, the absorbed energy directly drives evaporation to reduce energy loss. Therefore, PVA/CB-0.1/TA/Fe^{3+}-coated foam has the lowest equivalent evaporation enthalpy.

3.3. Antioil-Adhesion and Salt Resistance of Hydrogel-Coated Foam. The antioil-adhesion property of the evaporator is important for obtaining fresh water from sewage. Therefore, we detected the underwater−oil contact angle of the original foam and PVA/CB/TA/Fe^{3+}-coated foam. As shown in Figure 6a, the OCA of the pristine foam is about 148°, while PVA/CB-0.1/TA/Fe^{3+}-coated foam can reach 154°, indicating that the repellency of the foam to oils is

https://doi.org/10.1021/acsami.3c11299
ACS Appl. Mater. Interfaces XXXX, XXX, XXX−XXX

improved after modification. The underwater−oil adhesive test of the foam is shown in Figure 6b,c. When forcing the oil droplet (3 μL) to contact the surface of the hydrogel-coated foam and then slowly pulling it up, no oil was observed on the surface, indicating excellent antioil-adhesion performance (Figure 6b). When isooctane (dyed red) was jetted on the hydrogel-coated foam underwater, all oils could bounce off the foam without leaving a trace on the surface, showing good antioil-adhesion and self-cleaning performance (Figure 6c).

To further evaluate the antioil-adhesion performance of the foam, the solar water evaporation performance of PVA/CB/TA/Fe^{3+} and PVA/TA/Fe^{3+}-coated foams was evaluated using the sodium dodecyl sulfonate (SDS)-stabilized soybean oil-in-water emulsion under one sun irradiation. As shown in Figure 7a, the masses of PVA/CB/TA/Fe^{3+} and PVA/TA/Fe^{3+}-coated foams all decrease linearly in 1 h, showing excellent antioil-adhesion performance. The mass of PVA/CB/TA/Fe^{3+}-coated foam decreases faster than that of PVA/TA/Fe^{3+}-coated foam; therefore, the addition of CB improved the photothermal properties of the foam. The microscopic photographs in Figure 7b show that the emulsion before evaporation is milky white, and a large number of emulsified oil droplets are suspended in the emulsion. After evaporation, the collected liquid becomes clear and transparent, and no emulsified oil drops are observed (Figure 7c), indicating that the emulsified oils are effectively removed. The water molecules combined in the hydrogel can form a hydration layer, which effectively prevents the adhesion and fouling of oil.[43] Therefore, the hydrogel-coated foam has excellent antifouling performance and can realize the extraction of clean water from the emulsion.

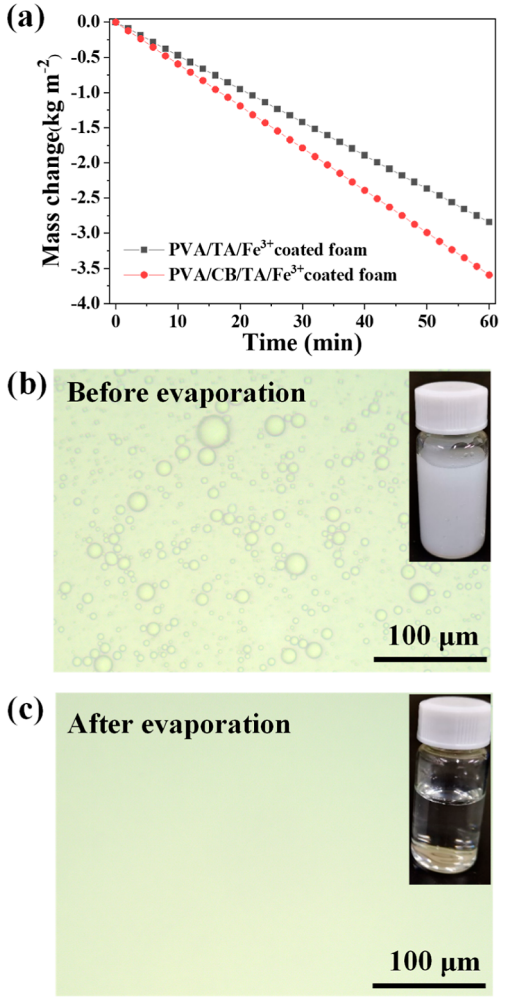

Figure 7. (a) Mass change curve of SDS-stabilized soybean oil-in-water emulsion in PVA/TA/Fe^{3+}- and PVA/CB/TA/Fe^{3+}-coated foams under 1 sun irradiation. Digital and microscopic photographs of SDS-stabilized soybean oil-in-water emulsion (b) before and (c) after evaporation.

Salt resistance is one of the most important factors that determines the practical application performance of the water evaporator.[44,45] The rapid water transport capacity can ensure salt diffusion back into water, which is essential to improving salt resistance during long-term use. As shown in Figure 8a, the filter paper (2 cm × 3 cm × 0.34 mm) on PVA/CB/TA/Fe^{3+}-coated foam can be completely wetted by water (dyed with rose red) in 5 s, indicating that the hydrogel-coated foam has rapid water transport capacity. The antisalt-fouling test of PVA/CB/TA/Fe^{3+}-coated foam is shown in Figure 8b, 1 g of salt crystal on the foam surface (4.5 cm × 4.5 cm) can completely disappear within 16 min, indicating that the salt is successfully dissolved through the pores of the hydrogel coating.

In order to further characterize the salt resistance of the foam, we investigated the continued water evaporation performance of the PVA/CB/TA/Fe^{3+}-coated foam in simulated seawater (3.5% NaCl) for 8 h. As shown in Figure 8c, the mass of seawater decreases linearly, and the water evaporation rate remains at about 3.37 kg m^{-2} h^{-1} under one sun. The digital photographs before and after evaporation show that no salt accumulation was found during the 8 h continuous test. We carried out the water evaporation experiment of PVA/CB/TA/Fe^{3+}-coated foam in actual seawater for 5 days. As shown in Figure 8d, the evaporation rate does not decrease obviously. The high porosity of porous foam and the excellent hydrophilicity of the hydrogel are conducive to the rapid diffusion of salt. Therefore, the hydrogel-coated foam demonstrates great potential in practical seawater purification.

3.4. Stability Tests of Hydrogel-Coated Foam. The stability of the hydrogel-coated foam is essential for its practical application. As shown in Figure 9a, the hydrogel-coated foam remains stable in acid−base solutions (pH = 2, 4, 6, 8, and 10), which meets most domestic and industrial wastewater treatment conditions. Moreover, the digital photographs show that the morphology of the hydrogel-coated foam does not change even after stirring at 1000 rpm for 24 h, indicating good mechanical stability (Figure 9b). As shown in Figure 9c, the height of the hydrogel-coated foam is almost the same as that of the original foam after 50 continuous compressions, which indicates that the foam has good recoverability. The good chemical and mechanical stability ensures the wide applicability of hydrogel-coated foam under different conditions.[46]

The outdoor experiment was conducted to evaluate the performance of evaporators in practical applications. The experiment was carried out on a sunny day in early September, from 9:30 a.m. to 16:30 p.m., on a self-made solar evaporator. The sunlight intensity and water evaporation performance of PVA/CB/TA/Fe^{3+}-coated foam in seawater are recorded in Figure 10. The average sunlight intensity is about 0.70 kW m^{-2}, while the average water evaporation rate is about 3.03 kg

https://doi.org/10.1021/acsami.3c11299
ACS Appl. Mater. Interfaces XXXX, XXX, XXX−XXX

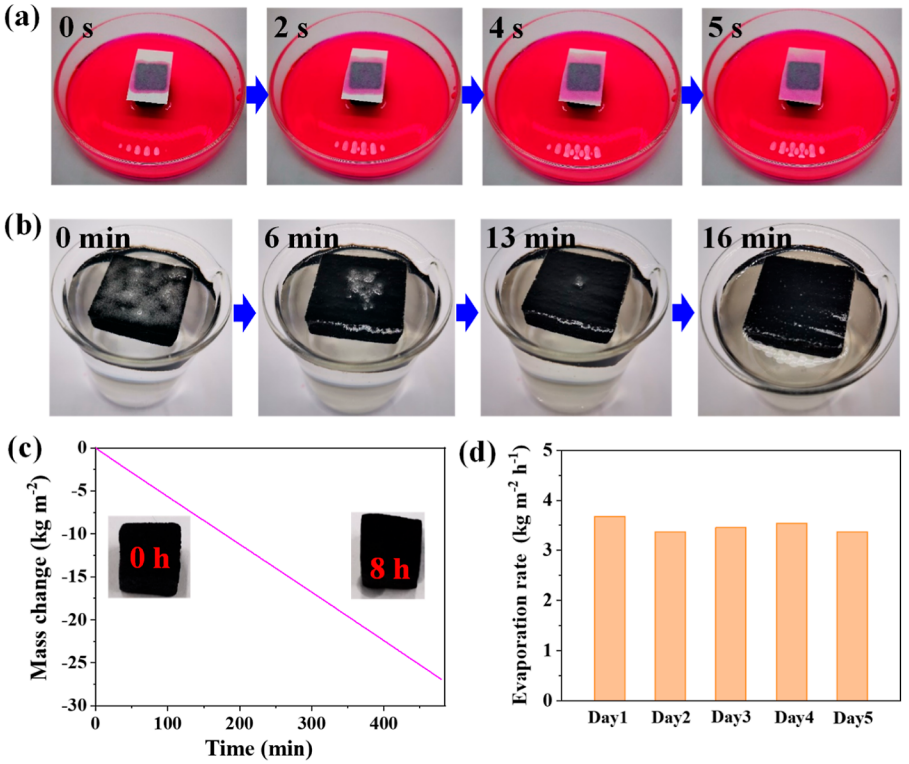

Figure 8. (a) The process of filter paper wetted by water dyed with rose red on PVA/CB/TA/Fe^{3+}-coated foam. (b) Antisalt-fouling test of PVA/CB/TA/Fe^{3+}-coated foam with 1 g NaCl on the surface. (c) Mass change curve of simulated seawater in PVA/CB/TA/Fe^{3+}-coated foam under 1 sun irradiation and the digital photographs of coated foam before and after evaporation. (d) Evaporation rate during the 5 day solar evaporation experiment using seawater.

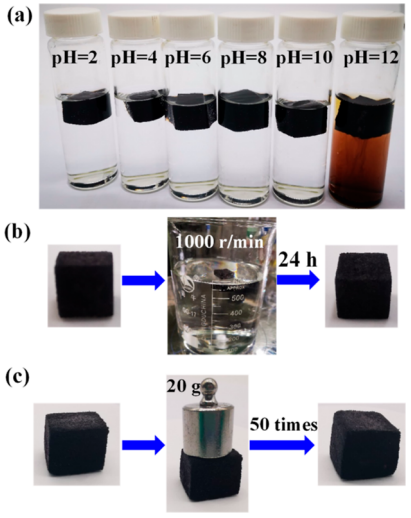

Figure 9. (a) Digital photographs of the hydrogel-coated foams after being immersed in acid−base solutions (pH = 2, 4, 6, 8, 10, and 12) for 2 h. (b) Digital photographs of the hydrogel-coated foam after being stirred in water for 24 h. (c) Digital photographs of the hydrogel-coated foam after being compressed 50 times.

m^{-2} h^{-1}, indicating that the hydrogel-coated foam has great potential in practical applications.

The comparison of evaporation performance between the hydrogel-coated foam and reported works is summarized in Table 1. Compared with other evaporators, the evaporation rate of PVA/CB/TA/Fe^{3+}-coated foam is higher, 3.64 kg m^{-2} h^{-1}, and the energy utilization efficiency is up to 90.13% (calculation process shown in Supporting Information note 3). This result demonstrates that the hydrogel-coated foam has great potential for practical water purification.

3.5. Solar Water Evaporation Mechanism. Based on the above results, the corresponding mechanism of solar water evaporation is described in Figure 11. The hydrogel-coated foam evaporator consists of a foam skeleton, a 3D hydrogel network formed by PVA and TA, and photothermal materials composed of CB and Fe^{3+}. When the sun shines on the evaporator, CB and Fe^{3+} work together to efficiently capture sunlight and convert solar energy to heat energy. Because Fe^{3+} is dispersed on the surface of the hydrogel coating, Fe^{3+} increases the light absorption capacity and realizes efficient capture of sunlight. As CB is dispersed in the hydrogel network, the absorbed heat energy is directly used to drive water evaporation in the hydrogel cross-linking network, thus reducing energy loss. At the same time, hydrophilic hydrogel significantly reduces the evaporation enthalpy of water, which decreases the energy requirements for water evaporation and further accelerates water evaporation. The 3D hydrogel network and porous skeleton structure provide a water supply channel to ensure continuous supply and rapid transportation of water. Therefore, the hydrogel-coated foam has excellent photothermal properties. In addition, due to the strong hydration of PVA and the high porosity of the foam, the hydrogel-coated foam shows excellent antioil-adhesion and salt resistance.

4. CONCLUSIONS

In this work, a hydrogel-coated evaporator was prepared via two-step immersion technology. The coating consists of a 3D hydrogel network formed by TA and PVA through a strong

https://doi.org/10.1021/acsami.3c11299
ACS Appl. Mater. Interfaces XXXX, XXX, XXX−XXX

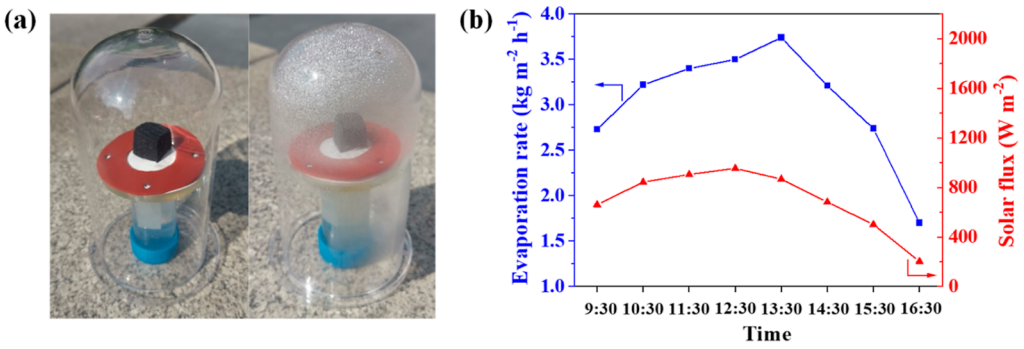

Figure 10. (a) Photographs of the evaporator used in the outdoor experiment. (b) Evaporation rate and solar flux during the outdoor experiment.

Table 1. Comparison of the Water Evaporation Performance with other Evaporators Reported in the Literature[a]

evaporators	irradiation intensity	evaporation rate (kg m^{-2} h^{-1})	energy utilization efficiency (%)	ref
PANI-SPPSU@PU	1 sun	1.91		47
PDMX/HPP aerogel	1 sun	2.62	93.6	48
PPy@PVA hydrogel	1 sun	2.64	96.3	49
Ca-ALG sponge	1 sun	3.10		9
AC/PVA/PAM	1 sun	2.33	84.7	42
PVA−PPy	1 sun	3.2	94	22
OTS patchy-surface hydrogel	1 sun	4.0	93	50
PVA/CB/TA/Fe^{3+}-coated foam	1 sun	3.64	90.1	this work

[a]PANI: polyaniline; SPPSU: sulfonated polyphenylsulfone; PU: polyurethane; PDMX: polydopamine-modified MXene; PPy: polypyrrole; Ca-ALG: calcium alginate; AC: activated carbon; PAM: polyacrylamide; and OTS: trichloro(octadecyl)silane.

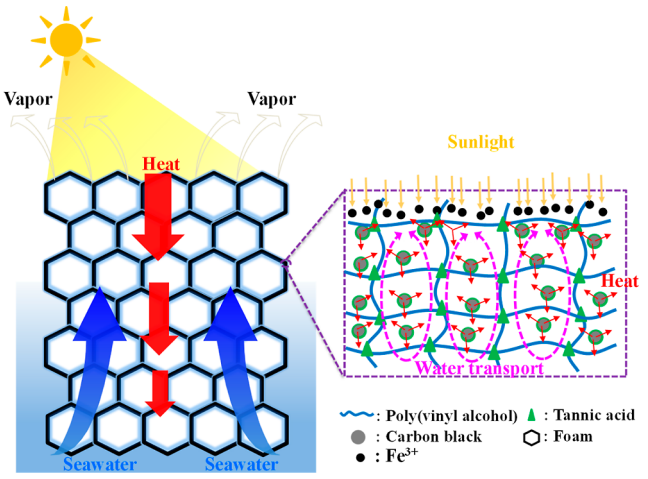

Figure 11. Schematic illustration of solar water purification.

hydrogen bond. CB is uniformly distributed within the hydrogel matrix with the assistance of the TA surface modifier. In addition, Fe^{3+} is deposited on the surface of the hydrogel coating through metal coordination with TA. Due to the synergistic effect of CB and Fe^{3+}, the hydrogel-coated foam exhibits excellent photothermal properties. The water evaporation rate reached 3.64 kg m^{-2} h^{-1} under 1 sun irradiation. Moreover, the hydrogel-coated foam shows excellent antioil-adhesion and salt resistance abilities. No salt accumulation is found during the 8 h continuous evaporation test of simulated seawater, and the mass of the SDS-stabilized soybean oil-in-water emulsion decreases linearly during the 1 h evaporation test. This study provides a facile way to design and manufacture high-performance solar-driven water evaporation materials and shows great potential for practical applications in the field of interfacial solar evaporation.

■ ASSOCIATED CONTENT

Supporting Information

The Supporting Information is available free of charge at https://pubs.acs.org/doi/10.1021/acsami.3c11299.

Experimental device for water evaporation; additional information for the preparation of hydrogel coating; XPS spectra for PVA/CB-0.1/TA/Fe^{3+}-coated foam; optimization of CB content in the coating; evaporation enthalpy of water in the foams; and calculation process of equivalent evaporation enthalpy and energy efficiency (PDF)

■ AUTHOR INFORMATION

Corresponding Author

Shenxiang Zhang − *College of Chemistry, Chemical Engineering and Materials Science; Jiangsu Key Laboratory of Advanced Functional Polymer Design and Application; Suzhou Key Laboratory of Macromolecular Design and Precision Synthesis, Soochow University, Suzhou 215123, China;* orcid.org/0000-0003-2857-333X; Email: sxzhang@suda.edu.cn

Authors

Xingzhen Zhang − *School of Chemistry and Chemical Engineering, Jiangsu Engineering Laboratory for Environment Functional Materials, Huaiyin Normal University, Huaian 223300, China; College of Chemistry, Chemical Engineering and Materials Science; Jiangsu Key Laboratory of Advanced Functional Polymer Design and Application; Suzhou Key Laboratory of Macromolecular Design and Precision Synthesis, Soochow University, Suzhou 215123, China*

Shouyong Zhou − *School of Chemistry and Chemical Engineering, Jiangsu Engineering Laboratory for Environment*

https://doi.org/10.1021/acsami.3c11299
ACS Appl. Mater. Interfaces XXXX, XXX, XXX−XXX

Functional Materials, Huaiyin Normal University, Huaian 223300, China

Zhigang Wang − *College of Chemistry, Chemical Engineering and Materials Science; Jiangsu Key Laboratory of Advanced Functional Polymer Design and Application; Suzhou Key Laboratory of Macromolecular Design and Precision Synthesis, Soochow University, Suzhou 215123, China*

Xian Wei − *College of Chemistry, Chemical Engineering and Materials Science; Jiangsu Key Laboratory of Advanced Functional Polymer Design and Application; Suzhou Key Laboratory of Macromolecular Design and Precision Synthesis, Soochow University, Suzhou 215123, China*

Jian Jin − *College of Chemistry, Chemical Engineering and Materials Science; Jiangsu Key Laboratory of Advanced Functional Polymer Design and Application; Suzhou Key Laboratory of Macromolecular Design and Precision Synthesis, Soochow University, Suzhou 215123, China; School of Chemistry and Chemical Engineering, Jiangsu Engineering Laboratory for Environment Functional Materials, Huaiyin Normal University, Huaian 223300, China;* orcid.org/0000-0003-0429-300X

Complete contact information is available at: https://pubs.acs.org/10.1021/acsami.3c11299

Author Contributions

S.X.Z. and X.Z. designed the project; X.Z., Z.W., and X.W. synthesized and characterized the photothermal materials; S.Y.Z. and J.J. provided suggestions and technical support. S.X.Z., X.Z., and J.J. wrote or/and edited the manuscript; J.J. supervised the project.

Notes

The authors declare no competing financial interest.

■ ACKNOWLEDGMENTS

The authors gratefully acknowledge support from the National Key Research and Development Program of China (2022YFB3805900, 2022YFB3805903), the National Natural Science Foundation of China (22208229, 21988102), the Natural Science Foundation of Jiangsu Province (BK20220501), and the Natural Science Research Program of Huaian (HAB202353).

■ REFERENCES

(1) Elsaid, K.; Kamil, M.; Sayed, E. T.; Abdelkareem, M. A.; Wilberforce, T.; Olabi, A. Environmental Impact of Desalination Technologies: A Review. *Sci. Total Environ.* **2020**, *748*, 141528.

(2) Jones, E.; Qadir, M.; van Vliet, M. T. H.; Smakhtin, V.; Kang, S. M. The State of Desalination and Brine Production: A Global Outlook. *Sci. Total Environ.* **2019**, *657*, 1343−1356.

(3) Khawaji, A. D.; Kutubkhanah, I. K.; Wie, J. M. Advances in Seawater Desalination Technologies. *Desalination* **2008**, *221*, 47−69.

(4) Elimelech, M.; Phillip, W. A. The Future of Seawater Desalination: Energy, Technology, and the Environment. *Science* **2011**, *333*, 712−717.

(5) Beh, E. S.; Benedict, M. A.; Desai, D.; Rivest, J. B. A Redox-Shuttled Electrochemical Method for Energy-Efficient Separation of Salt from Water. *ACS Sustain. Chem. Eng.* **2019**, *7*, 13411−13417.

(6) Zhou, X. Y.; Zhao, F.; Guo, Y. H.; Zhang, Y.; Yu, G. H. A Hydrogel-Based Antifouling Solar Evaporator for Highly Efficient Water Desalination. *Energy Environ. Sci.* **2018**, *11*, 1985−1992.

(7) Qi, D. P.; Liu, Y.; Liu, Y. B.; Liu, Z. Y.; Luo, Y. F.; Xu, H. B.; Zhou, X.; Zhang, J. J.; Yang, H.; Wang, W.; Chen, X. D. Polymeric Membranes with Selective Solution-Diffusion for Intercepting Volatile Organic Compounds during Solar-Driven Water Remediation. *Adv. Mater.* **2020**, *32*, 2004401.

(8) Yang, H.; Sun, Y. H.; Peng, M. W.; Cai, M. J.; Zhao, B.; Li, D.; Liang, Z. Q.; Jiang, L. Tailoring the Salt Transport Flux of Solar Evaporators for a Highly Effective Salt-Resistant Desalination with High Productivity. *ACS Nano* **2022**, *16*, 2511−2520.

(9) Wu, S. L.; Lu, F.; Deng, R.; Quan, L. N.; Yang, H. C.; Xu, Z. K. Solar-Driven Evaporators with Thin-Film-Composite Architecture Inspired by Plant Roots for Treating Concentrated Nano-/Submicrometer Emulsions. *ACS Appl. Mater. Interfaces* **2022**, *14*, 51555−51563.

(10) Li, D. D.; Zhou, Q. X.; Wang, G.; Zhao, H.; Ma, S. H.; Leng, K. Y.; Wang, Y.; Bai, J. B. Assembly of Janus Complex with Low-Cost and Salt Rejection for Solar-Thermal Water Evaporation. *J. Mater. Sci.* **2020**, *55*, 15551−15561.

(11) Kuang, Y. D.; Chen, C. J.; He, S. M.; Hitz, E. M.; Wang, Y. L.; Gan, W. T.; Mi, R. Y.; Hu, L. B. A High-Performance Self-Regenerating Solar Evaporator for Continuous Water Desalination. *Adv. Mater.* **2019**, *31*, 1900498.

(12) Xu, W. C.; Hu, X. Z.; Zhuang, S. D.; Wang, Y. X.; Li, X. Q.; Zhou, L.; Zhu, S. N.; Zhu, J. Flexible and Salt Resistant Janus Absorbers by Electrospinning for Stable and Efficient Solar Desalination. *Adv. Energy Mater.* **2018**, *8*, 1702884.

(13) Wu, S. L.; Quan, L. N.; Huang, Y. T.; Li, Y. T.; Yang, H. C.; Darling, S. B. Suspended Membrane Evaporators Integrating Environmental and Solar Evaporation for Oily Wastewater Purification. *ACS Appl. Mater. Interfaces* **2021**, *13*, 39513−39522.

(14) Wang, Z. B.; Guo, P.; Heng, L. P.; Jiang, L. Nano/submicrometer-Emulsion Oily Wastewater Treatment Inspired by Plant Transpiration. *Matter* **2021**, *4*, 1274−1286.

(15) Zhou, X. Y.; Guo, Y. H.; Zhao, F.; Yu, G. H. Hydrogels as an Emerging Material Platform for Solar Water Purification. *Acc. Chem. Res.* **2019**, *52*, 3244−3253.

(16) Zhao, F.; Bae, J.; Zhou, X. Y.; Guo, Y. H.; Yu, G. H. Nanostructured Functional Hydrogels as an Emerging Platform for Advanced Energy Technologies. *Adv. Mater.* **2018**, *30*, 1801796.

(17) Zhang, Y. S.; Khademhosseini, A. Advances in Engineering Hydrogels. *Science* **2017**, *356*, No. eaaf3627.

(18) Peng, B. L.; Lyu, Q. Q.; Gao, Y. J.; Li, M. M.; Xie, G.; Xie, Z. J.; Zhang, H. C.; Ren, J. L.; Zhu, J. T.; Zhang, L. B.; Wang, P. Composite Polyelectrolyte Photothermal Hydrogel with Anti-biofouling and Antibacterial Properties for the Real-World Application of Solar Steam Generation. *ACS Appl. Mater. Interfaces* **2022**, *14*, 16546−16557.

(19) Cao, S.; Jiang, J. Y.; Tian, Q. Y.; Guo, C.; Wang, X. Z.; Dai, K.; Xu, Q. Building of Multifunctional and Hierarchical H_xMoO_3/PNIPAM Hydrogel for High-Efficiency Solar Vapor Generation. *Green Energy Environ.* **2022**, *7*, 1006−1013.

(20) Hu, G. Y.; Cao, Y.; Huang, M. Y.; Wu, Q.; Zhang, K. X.; Lai, X. Y.; Tu, J. C.; Tian, C.; Liu, J.; Huang, W.; Ding, L. Salt-Resistant Carbon Nanotubes/Polyvinyl Alcohol Hybrid Gels with Tunable Water Transport for High-Efficiency and Long-Term Solar Steam Generation. *Energy Technol.* **2020**, *8*, 1900721.

(21) Guo, Y. H.; Zhou, X. Y.; Zhao, F.; Bae, J.; Rosenberger, B.; Yu, G. H. Synergistic Energy Nanoconfinement and Water Activation in Hydrogels for Efficient Solar Water Desalination. *ACS Nano* **2019**, *13*, 7913−7919.

(22) Zhao, F.; Zhou, X. Y.; Shi, Y.; Qian, X.; Alexander, M.; Zhao, X. P.; Mendez, S.; Yang, R. G.; Qu, L. T.; Yu, G. H. Highly Efficient Solar Vapour Generation via Hierarchically Nanostructured gels. *Nat. Nanotechnol.* **2018**, *13*, 489−495.

(23) Xu, T.; Xu, Y. X.; Wang, J. Y.; Lu, H. J.; Liu, W. P.; Wang, J. Sustainable Self-Cleaning Evaporator for Long-Term Solar Desalination Using Gradient Structure Tailored Hydrogel. *Chem. Eng. J.* **2021**, *415*, 128893.

(24) Wang, Z. X.; Wu, X. C.; Dong, J. M.; Yang, X. H.; He, F.; Peng, S. Q.; Li, Y. X. Porifera-Inspired Cost-Effective and Scalable "Porous Hydrogel Sponge" for Durable and Highly Efficient Solar-Driven Desalination. *Chem. Eng. J.* **2022**, *427*, 130905.

(25) Sheng, C. M.; Yang, N.; Yan, Y. T.; Shen, X. P.; Jin, C. D.; Wang, Z.; Sun, Q. F. Bamboo Decorated with Plasmonic Nanoparticles for Efficient Solar Steam Generation. *Appl. Therm. Eng.* **2020**, *167*, 114712.
(26) Wang, X. Z.; He, Y. R.; Hu, Y. W.; Jin, G. R.; Jiang, B. C.; Huang, Y. M. Photothermal-Conversion-Enhanced Photocatalytic Activity of Flower-like CuS Superparticles Under Solar Light Irradiation. *Sol. Energy* **2018**, *170*, 586−593.
(27) Wu, X.; Robson, M. E.; Phelps, J. L.; Tan, J. S.; Shao, B.; Owens, G.; Xu, H. L. A Flexible Photothermal Cotton-CuS Nanocage-Agarose Aerogel Towards Portable Solar Steam Generation. *Nano Energy* **2019**, *56*, 708−715.
(28) Yao, Z. P.; Yu, K. L.; Pan, M. Y.; Xu, H. B.; Zhao, T. Q.; Jiang, Z. H. A Mechanically Durable, Excellent Recyclable 3D Hierarchical Ni_3S_2@Ni Foam Photothermal Membrane. *Green Energy Environ.* **2022**, *7*, 492−499.
(29) Dao, V. D.; Choi, H. S. Carbon-Based Sunlight Absorbers in Solar-Driven Steam Generation Devices. *Glob. Chall* **2018**, *2*, 1700094.
(30) Wang, Y. C.; Zhang, L. B.; Wang, P. Self-Floating Carbon Nanotube Membrane on Macroporous Silica Substrate for Highly Efficient Solar-Driven Interfacial Water Evaporation. *ACS Sustain. Chem. Eng.* **2016**, *4*, 1223−1230.
(31) Yang, Y.; Zhao, R. Q.; Zhang, T. F.; Zhao, K.; Xiao, P. S.; Ma, Y. F.; Ajayan, P. M.; Shi, G. Q.; Chen, Y. S. Graphene-Based Standalone Solar Energy Converter for Water Desalination and Purification. *ACS Nano* **2018**, *12*, 829−835.
(32) Li, Y. L.; Cui, X. X.; Zhao, M. Y.; Xu, Y. S.; Chen, L. L.; Cao, Z. J.; Yang, S. G.; Wang, Y. Facile Preparation of a Robust Porous Photothermal Membrane with Antibacterial Activity for Efficient Solar-Driven Interfacial Water Evaporation. *J. Mater. Chem. A* **2019**, *7*, 704−710.
(33) Holloway, J. L.; Lowman, A. M.; Palmese, G. R. The Role of Crystallization and Phase Separation in the Formation of Physically Cross-Linked PVA Hydrogels. *Soft Matter* **2013**, *9*, 826−833.
(34) Di Turo, F.; Matricardi, P.; Di Meo, C.; Mazzei, F.; Favero, G.; Zane, D. PVA Hydrogel as Polymer Electrolyte for Electrochemical Impedance Analysis on Archaeological Metals. *J. Cult. Herit.* **2019**, *37*, 113−120.
(35) Azadi, S.; Peng, S. H.; Moshizi, S. A.; Asadnia, M.; Xu, J. T.; Park, I.; Wang, C. H.; Wu, S. Y. Biocompatible and Highly Stretchable PVA/AgNWs Hydrogel Strain Sensors for Human Motion Detection. *Adv. Mater. Technol.* **2020**, *5*, 2000426.
(36) Wang, M. H.; Bai, J. Z.; Shao, K.; Tang, W. W.; Zhao, X. L.; Lin, D. H.; Huang, S.; Chen, C.; Ding, Z.; Ye, J. Y. Poly(vinyl alcohol) Hydrogels: The Old and New Functional Materials. *Int. J. Polym. Sci.* **2021**, *2021*, 1−16.
(37) Niu, W. W.; Zhu, Y. L.; Wang, R.; Lu, Z. Y.; Liu, X. K.; Sun, J. Q. Remalleable, Healable, and Highly Sustainable Supramolecular Polymeric Materials Combining Superhigh Strength and Ultrahigh Toughness. *ACS Appl. Mater. Interfaces* **2020**, *12*, 30805−30814.
(38) Bai, Z. X.; Jia, K.; Liu, C. C.; Wang, L. L.; Lin, G.; Huang, Y. M.; Liu, S. N.; Liu, X. B. A Solvent Regulated Hydrogen Bond Crosslinking Strategy to Prepare Robust Hydrogel Paint for Oil/Water Separation. *Adv. Funct. Mater.* **2021**, *31*, 2104701.
(39) Wang, Z. X.; Wu, X. C.; He, F.; Peng, S. Q.; Li, Y. X. Confinement Capillarity of Thin Coating for Boosting Solar-Driven Water Evaporation. *Adv. Funct. Mater.* **2021**, *31*, 2011114.
(40) He, F.; Han, M. C.; Zhang, J.; Wang, Z. X.; Wu, X. C.; Zhou, Y. Y.; Jiang, L. F.; Peng, S. Q.; Li, Y. X. A Simple, Mild and Versatile Method for Preparation of Photothermal Woods Toward Highly Efficient Solar Steam Generation. *Nano Energy* **2020**, *71*, 104650.
(41) Chu, A.; Yang, M.; Chen, J.; Zhao, J.; Fang, J.; Yang, Z.; Li, H. Biomass-Enhanced Janus Sponge-like Hydrogel with Salt Resistance and High Strength for Efficient Solar Desalination. *Green Energy Environ.* **2023**, 30.
(42) Chu, A. Q.; Yang, M.; Yang, H. D.; Shi, X. Q.; Chen, J. L.; Fang, J.; Wang, Z. Y.; Li, H. Sustainable Self-Cleaning Evaporators for Highly Efficient Solar Desalination Using a Highly Elastic Sponge-like Hydrogel. *ACS Appl. Mater. Interfaces* **2022**, *14*, 36116−36131.
(43) Gao, S. J.; Sun, J. C.; Liu, P. P.; Zhang, F.; Zhang, W. B.; Yuan, S. L.; Li, J. Y.; Jin, J. A Robust Polyionized Hydrogel with an Unprecedented Underwater Anti-Crude-Oil-Adhesion Property. *Adv. Mater.* **2016**, *28*, 5307−5314.
(44) Nawaz, F.; Yang, Y. W.; Zhao, S. H.; Sheng, M. H.; Pan, C.; Que, W. X. Innovative Salt-Blocking Technologies of Photothermal Materials in Solar-Driven Interfacial Desalination. *J. Mater. Chem. A* **2021**, *9*, 16233−16254.
(45) Wu, S. L.; Chen, H. L.; Wang, H. L.; Chen, X. L.; Yang, H. C.; Darling, S. B. Solar-Driven Evaporators for Water Treatment: Challenges and Opportunities. *Environ. Sci.: Water Res.* **2021**, *7*, 24−39.
(46) Gong, F.; Li, H.; Wang, W. B.; Huang, J. G.; Xia, D. D.; Liao, J. X.; Wu, M. Q.; Papavassiliou, D. V. Scalable, Eco-friendly and Ultrafast Solar Steam Generators Based on One-step Melamine-Derived Carbon Sponges Toward Water Purification. *Nano Energy* **2019**, *58*, 322−330.
(47) Zhao, X.; Dong, J.; Yu, X.; Liu, L.; Liu, J.; Pan, J. Bioinspired Photothermal Polyaniline Composite Polyurethane Sponge: Interlayer Engineering for High-Concentration Seawater Desalination. *Sep. Purif. Technol.* **2023**, *311*, 123181.
(48) Wang, Z. Y.; Zhu, Y. J.; Chen, Y. Q.; Yu, H. P.; Xiong, Z. C. Bioinspired Aerogel with Vertically Ordered Channels and Low Water Evaporation Enthalpy for High-Efficiency Salt-Rejecting Solar Seawater Desalination and Wastewater Purification. *Small* **2023**, *19*, No. e2206917.
(49) Zhao, X.; Chen, Y. Y.; Yin, Y.; Zou, L. Q.; Chen, Q. Y.; Liu, K.; Lin, P. C.; Su, H.; Chen, Y. Janus Polypyrrole Nanobelt@Polyvinyl Alcohol Hydrogel Evaporator for Robust Solar-Thermal Seawater Desalination and Sewage Purification. *ACS Appl. Mater. Interfaces* **2021**, *13*, 46717−46726.
(50) Guo, Y.; Zhao, X.; Zhao, F.; Jiao, Z.; Zhou, X.; Yu, G. Tailoring Surface Wetting States for Ultrafast Solar-Driven Water Evaporation. *Energy Environ. Sci.* **2020**, *13*, 2087−2095.

https://doi.org/10.1021/acsami.3c11299
ACS Appl. Mater. Interfaces XXXX, XXX, XXX−XXX